Hindawi
Wireless Communications and Mobile Computing
Volume 2021, Article ID 6670591, 16 pages
https://doi.org/10.1155/2021/6670591

Research Article

Edge Computing- and H_∞-Switching-Based Networked Control for Frequency Control in Multi-Microgrids with Time Delays

Peng Yang[1], **Wei Guo**[2], **Guanghua Wu**[2], **Cong Wang**[3], **Kai Zhang**[1] and **Ran Zhang**[1]

[1]*State Grid Hebei Electric Power Co., LTD., Shijiazhuang 050021, China*
[2]*Market Service Center, State Grid Hebei Electric Power Co., LTD., Shijiazhuang 050021, China*
[3]*Shijiazhuang Power Supply Company, State Grid Hebei Electric Power Co., LTD., Shijiazhuang 050021, China*

Correspondence should be addressed to Wei Guo; yxzx_guow@he.sgcc.com.cn

Received 14 October 2020; Revised 26 November 2020; Accepted 10 December 2020; Published 6 January 2021

Academic Editor: Mohammad R. Khosravi

The frequency stability of multi-microgrids is easily affected by random load fluctuations and intermittent renewable resources. Additionally, geographically distributed generation equipment usually cannot adopt the "point-to-point" dedicated communication scheme to realize the information exchange considering the construction and computation costs. Therefore, a H_∞-switching frequency control strategy for multi-microgrids based on edge computing framework is proposed in this paper. Firstly, an edge computing device is set up in each microgrid to collect the operation statuses of local participating equipment and generate the control instructions to ensure the real-time local frequency stability. Secondly, the multihop data transmission process in edge computing environment is described as a cascade queuing model. Then, the frequency control system in each microgrid is described as a switching model dependent on the varying time delays. Finally, via constructing a Lyapunov function, the constraints of the controller gains ensuring the H_∞-damping performance for external load demands and the renewable outputs are derived at the same time. Simulation results show that compared with the traditional centralized control schemes, the peak value of our proposed edge computing framework is reduced by 32.51% compared with the traditional centralized control scheme. Moreover, under the same edge computing framework, the integral of absolute error (IAE) of frequency with the proposed H_∞ control strategy can be reduced by 37.19% at least. Therefore, a better transient performance can be obtained with our proposed method.

1. Introduction

The microgrid is usually used to supply power for the rural areas, islands, and so on. Integrating multi-microgrids into the power systems can effectively address the contradiction between the load growth and the power infrastructure expansion [1]. The main feature of the multi-microgrids is that each microgrid integrates the high-proportional renewable generators and exchanges active power with the neighbouring microgrids through tie lines [2, 3]. However, the uncertainties in renewable outputs and load demands usually cause the active power mismatch between the supply and demand in the power systems. Correspondingly, the frequency in each microgrid will deviate from the rated value [4]. To maintain the real-time balance of active power supply and demand at the rated frequency point, the global operation statuses of each microgrid are usually collected in traditional centralized control strategies while the output adjustment instructions are sent out to the participating equipment including synchronous generators and energy storage systems in each microgrid [5, 6]. However, because there is only one centralized control center in the whole power system, the computing burden in the control center is usually heavy. Besides, if the number of interconnected microgrids is too large, there will be significant disadvantages of the centralized control strategies in reliability and construction costs of

communication facilities [7]. In addition, too many interconnected microgrids will cause the dimensional disaster in traditional centralized frequency control schemes, which may lead to no solution for the controller gains [8].

With the rapid development of Internet of things and edge computing technologies, using decentralized control structure and sharing communication networks have attracted considerable attentions. Different from the traditional centralized control scheme, in edge computing framework, the edge computing device with data storing, processing, and analysing capabilities is set up in each microgrid which is considered as the local control center to realize the local power balance at the rated frequency point [9, 10]. Since the edge computing device is closer to the participating equipment, the corresponding transmission delay can be shorten compared with the traditional centralized control schemes. However, it still should be noted that the influences of stochastic time delays and packet losses cannot be ignored in the controller design process. The numerical results in [11, 12] show that even the millisecond-level time delay may cause the frequency deviation exceeding the allowable ranges or even instability risk. Hence, the literatures concerning the delay/packet loss-dependent frequency control in multi-microgrids can be divided into the following two categories.

1.1. Delay Margin Calculation. In this context, the controller parameters for frequency stabilization are firstly determined. Then, the maximum allowable time delay that guarantees frequency deviation within the permitted ranges is calculated. For example, the analytical relationship between delay margin and controller gain is derived by constructing a Lyapunov function in [13]. Similarly, in [14], a stability criterion of frequency control system concerning the controller parameters and delay margin is proposed on the basis of the regular polynomial method. In [15], an event-triggered communication mechanism is proposed for the frequency control in power systems. Only when the frequency deviation exceeds the preset threshold, the update of control instructions can be triggered. The authors in [15] also strictly proved the analytical relationship among controller parameters, delay margin, and the triggering threshold. However, the disadvantage of above studies is that the controller parameters must be given in advance. Therefore, the optimal dynamic performance of frequency control systems cannot be guaranteed when the power system suffers from the varying time delays. In addition, when the actual transmission delays of the packets exceed the allowable delay margin, the frequency control system will be instable.

1.2. Delay/Packet Loss-Dependent Controller Design. In this context, the controller parameters are obtained according to the actual transmission delays. Therefore, the control performance of the frequency control system can be improved effectively. For example, in [16], queuing theory is adopted to calculate the delay ranges in power systems. Besides, a decentralized control strategy based on linear matrix inequality-linear quadratic regulator (LMI-LQR) is proposed to guarantee the closed-loop asymptotic stability in the maximum delay case. The effects of packet losses on the control performance have not been discussed in [16]. In [17], a robust model predictive control (MPC) method is proposed to tackle the frequency stability problem in power systems with stochastic time delays. However, the MPC method needs to store continuous historical data to generate the control instructions. Moreover, the instruction calculation in MPC also introduces additional delays. In [18], a decentralized robust sliding control strategy is proposed to damping the frequency deviations in power systems with time delays. However, the external active power distributions from load demands and renewable outputs are assumed to be known in advance during the sliding surface construction process. In fact, it is the uncertainties of load demand and renewable outputs that lead to the frequency deviation from the rated value, so the practicability of the method in [18] is indeed open to debate. Furthermore, the current studies mainly pay close attention to the closed-loop asymptotic stability in the maximum transmission delay case. The dynamic performance during frequency restoration process is sacrificed to some extent.

Based on the above analysis, a H_∞-switching control strategy for frequency stability in multi-microgrids based on edge computing framework is proposed in this paper. The main contributions are given as follows:

(1) An edge computing framework for frequency stability in multi-microgrids is proposed. Rather than the traditional centralized control schemes which require global operation statuses of all the microgrids, the edge computing device is set up in each microgrid to be responsible for maintaining the local power balance between supply and demand sides at the rated frequency point. Correspondingly, the lighter communication burden and lower computation cost can be realized

(2) Based on the queuing theory, the analytical relationship between the transmission delay and the network parameters such as packet size, transmission rate, and transmission hops in the process of multihop data transmission process under the edge computing framework is calculated. Then, the dynamics of frequency control system in each microgrid are further described as a switching model which depends on the time-varying delay. Hence, the mapping relationship between time-varying delay and dynamic frequency deviation response can be revealed more clearly

(3) By constructing a Lyapunov function, a stability criterion of the closed-loop delay-dependent frequency control system with H_∞-damping performance for external power disturbances is strictly derived. Furthermore, by aiming at minimizing the integral of absolute error (IAE) of the frequency in each microgrid, a constrained controller optimization algorithm is proposed. Then, the dynamic performance during frequency restoration process can be improved

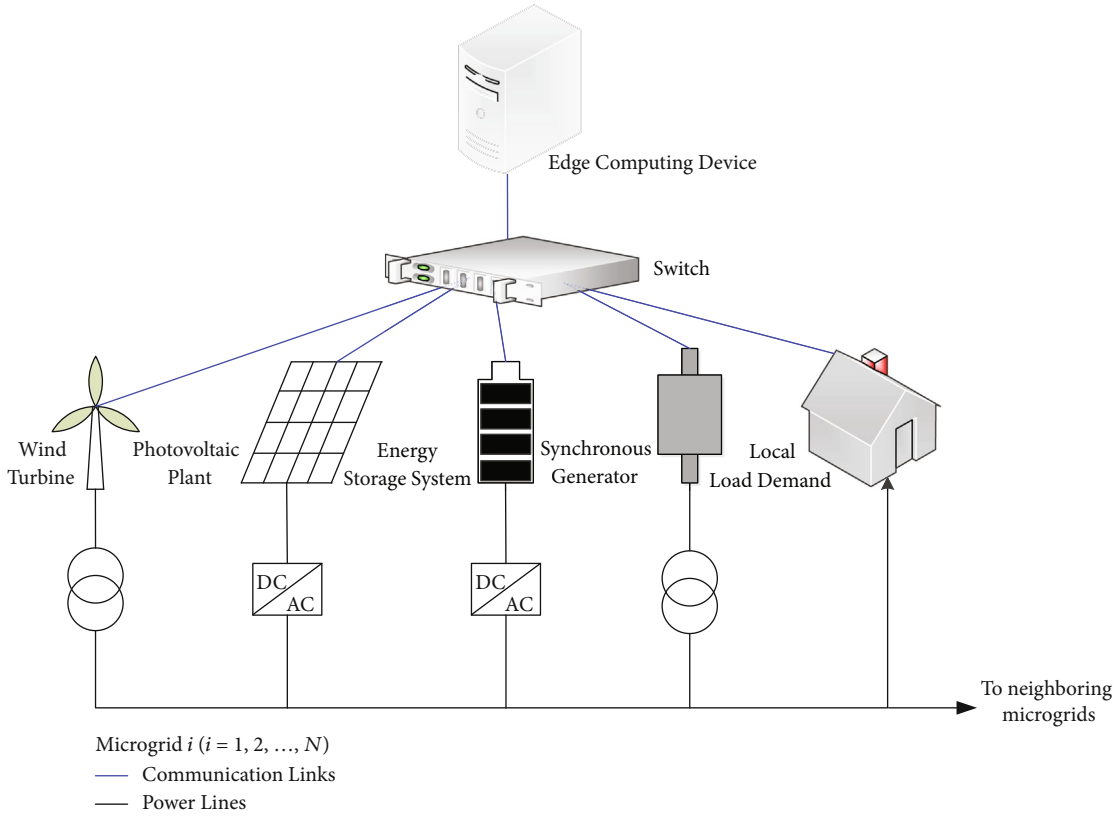

Figure 1: Framework of multi-microgrids with edge computing framework.

The rest is organized as follows. State-space model for frequency control system in each microgrid is established in Section 2. In Section 3, the relationships among transmission delay and key network parameters are investigated. The dynamics of closed-loop frequency control system with time-varying delays are discussed in Section 4. In Section 5, an optimization method combined with iterative linear matrix inequality and heuristic algorithm is proposed. Simulations are discussed in Section 6. Finally, conclusions are given in Section 7.

2. State-Space Model of Frequency Control in Multi-Microgrids Based on Edge Computing Framework

The power resources in multi-microgrids mainly contain synchronous generators, renewable generators (such as wind turbines and photovoltaic cells), and energy storage systems. Due to the uncertain fluctuations of renewable outputs and load demands, the frequency may deviate from the rated value. Hence, it is required to timely adjust the outputs of synchronous generators and energy storage systems to maintain real-time power balance between supply and demand at the rated frequency point [19, 20]. Considering that there exist the heavy communication and computation burdens in the traditional centralized control scheme which requires global operation statuses of all the microgrids, in this paper, a frequency control strategy based on edge computing framework is proposed. As shown in Figure 1, the local operating statuses are transmitted to the edge computing device installed in each microgrid. In other words, in our proposed edge computing framework, an edge computing device considered as the local control center is set up in each microgrid. Since the local controller is closer to the participating equipment and the corresponding control structure is simpler, lighter communication burden and lower computation cost can be realized. Similar to the centralized scheme, the function of the edge computing device is sending the active power output commands of synchronous generators and energy storage systems and then restoring the frequency to the rated value. Note that the edge computing devices and devices participating in frequency control are geographically dispersed; the uploading of operation statuses usually relays on the sharing communication network. Hence, there exist time delay and packet loss problems during the data transmission process. In this section, the state-space model of frequency control system in each microgrid is firstly discussed. The effects of time delay and packet loss on the dynamics of frequency control system will be analysed in the next sections.

Let the number of microgrids in a multi-microgrid be N. For the i-th ($i = 1, 2, \cdots, N$) microgrid, the equivalent block diagram of the frequency control system is shown in Figure 2. Moreover, let the number of synchronous generators and energy storage systems in i-th microgrid be M_{SG_i} and M_{ESS_i}, respectively. Therefore, the dynamics of the frequency control system in i-th microgrid satisfy [4]

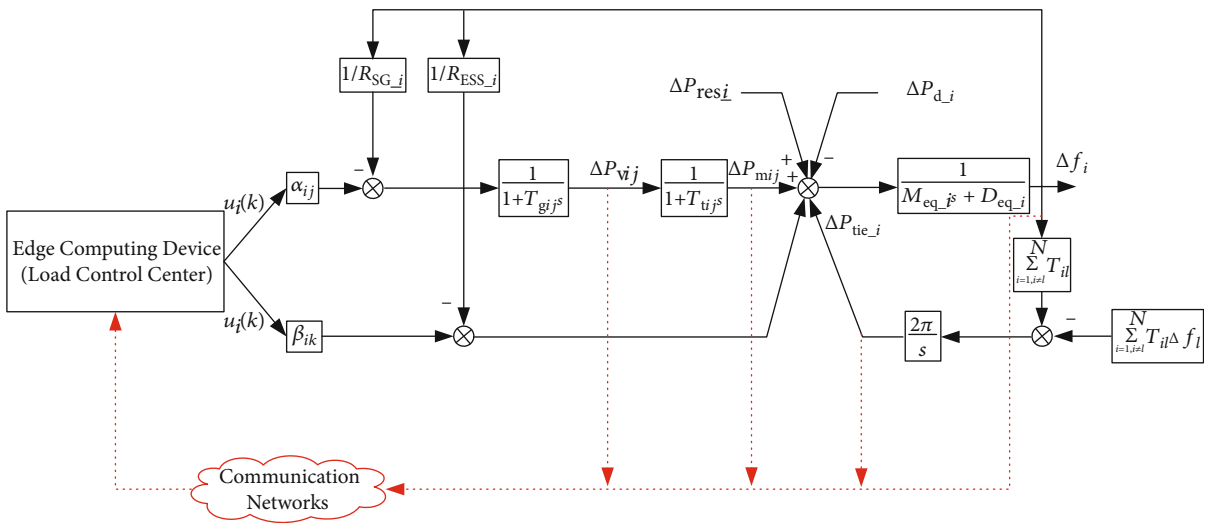

Figure 2: Control block of networked frequency control system.

$$\begin{cases} \dfrac{d}{dt}\Delta P_{vij} = -\dfrac{1}{T_{gij}}\Delta P_{vij} + \dfrac{1}{T_{gij}}\left(\alpha_{ij}u_i - \dfrac{1}{R_{ij}}\Delta f_i\right), \\ \dfrac{d}{dt}\Delta P_{mij} = -\dfrac{1}{T_{tij}}\Delta P_{mij} + \dfrac{1}{T_{tij}}\Delta P_{vij}, \\ \dfrac{d}{dt}\Delta P_{tie\_i} = 2\pi\sum\limits_{i=1,i\neq l}^{N} T_{il}(\Delta f_i - \Delta f_l), \\ \dfrac{d}{dt}\Delta f_i = -\dfrac{D_{eq\_i}}{M_{eq\_i}}\Delta f_i + \dfrac{1}{M_{eq\_i}}\left(\sum\limits_{j=1}^{M_{SG\_i}}\Delta P_{mij} + \Delta P_{res\_i} + \sum\limits_{k=1}^{M_{ESS\_i}}\Delta P_{ESS\_ik} - \Delta P_{di} - \Delta P_{tie\_i}\right), \\ \Delta P_{ESS\_ik} = \beta_{ik}u_i - \dfrac{1}{R_{ESS\_ik}}\Delta f_i, \end{cases} \tag{1}$$

where ΔP_{vij} is the valve opening of the j-th synchronous generator; ΔP_{mij} is the mechanical output power of the j-th synchronous generator; ΔP_{tie_i} is the tie line power fluctuation in i-th microgrid; Δf_i and Δf_l are the frequency deviations in the i-th and l-th microgrids, respectively; T_{il} is the synchronization coefficient of the tie line between the i-th and l-th microgrids; T_{gij} and T_{tij} are the time constants of governor and turbine in the j-th synchronous generator; R_{ij} and R_{ESS_ik} are the drooping coefficients of the j-th synchronous generator and k-th energy storage system, respectively; ΔP_{ESS_ik} is the active output power of the k-th energy storage system; ΔP_{di} and ΔP_{res_i} are the fluctuations of load demand and renewable output in the i-th microgrids, respectively; M_{eq_i} and D_{eq_i} are the equivalent inertia and damping coefficient of the i-th microgrids, respectively; α_{ij} and β_{ik} are the participation factors of the j-th synchronous generator and k-th energy storage system, respectively, and satisfy

$$\sum_{j=1}^{M_{SG\_i}}\alpha_{ij} + \sum_{k=1}^{M_{ESS\_i}}\beta_{ik} = 1. \tag{2}$$

By defining the state vector as $X_i = [\Delta f_i, \Delta P_{tie\_i}, \Delta P_{mi1}, \cdots, \Delta P_{miM_{SG\_i}}, \Delta P_{vi1}, \cdots, \Delta P_{viM_{SG\_i}}]^T$, the state-space model of the frequency control system in the i-th microgrid is given by

$$\begin{cases} \dfrac{d}{dt}X_i(t) = A_iX_i(t) + B_iu_i(t) + H_iw_i(t), \\ Y_i(t) = C_iX_i(t), \end{cases} \tag{3}$$

where

$$A_i = \begin{bmatrix} -\frac{D_{\text{eq\_}i}}{M_{\text{eq\_}i}} - \frac{1}{M_{\text{eq\_}i}} \sum_{k=1}^{M_{\text{ESS\_}i}} \frac{1}{R_{\text{ESS\_}ik}} & -\frac{1}{M_{\text{eq\_}i}} & \frac{1}{M_{\text{eq\_}i}} & \cdots & \frac{1}{M_{\text{eq\_}i}} & 0 & \cdots & 0 \\ 2\pi \sum_{i=1, i\neq l}^{N} T_{il} \Delta f_i & 0 & 0 & \cdots & 0 & 0 & \cdots & 0 \\ 0 & 0 & -\frac{1}{T_{ti1}} & \cdots & 0 & \frac{1}{T_{ti1}} & \cdots & 0 \\ \vdots & \vdots & \vdots & \ddots & \vdots & \vdots & \ddots & \vdots \\ 0 & 0 & 0 & \cdots & -\frac{1}{T_{tiM_{\text{SG\_}i}}} & 0 & \cdots & \frac{1}{T_{tiM_{\text{SG\_}i}}} \\ \frac{1}{T_{gi1} R_{i1}} & 0 & 0 & \cdots & 0 & -\frac{1}{T_{gi1}} & \cdots & 0 \\ \vdots & \vdots & \vdots & \ddots & \vdots & \vdots & \ddots & \vdots \\ \frac{1}{T_{giM_{\text{SG\_}i}} R_{iM_{\text{SG\_}i}}} & 0 & 0 & \cdots & 0 & 0 & \cdots & -\frac{1}{T_{giM_{\text{SG\_}i}}} \end{bmatrix},$$

$$B_i = \begin{bmatrix} \frac{\sum_{k=1}^{M_{\text{ESS\_}i}} \beta_{ik}}{M_{\text{eq\_}i}} \\ 0 \\ 0 \\ \vdots \\ 0 \\ \frac{\alpha_{i1}}{T_{gi1} R_{i1}} \\ \vdots \\ \frac{\alpha_{iM_{\text{SG\_}i}}}{T_{giM_{\text{SG\_}i}}} \end{bmatrix}, H_i = \begin{bmatrix} -\frac{1}{M_{\text{eq\_}i}} & 0 \\ 0 & -2\pi \\ 0 & 0 \\ \vdots & \vdots \\ 0 & 0 \\ 0 & 0 \\ \vdots & \vdots \\ 0 & 0 \end{bmatrix}, C_i = \begin{bmatrix} 1 \\ 0 \\ 0 \\ \vdots \\ 0 \\ 0 \\ \vdots \\ 0 \end{bmatrix}^{\text{T}}, w_i = \begin{bmatrix} \Delta P_{\text{d}i} - \Delta P_{\text{res\_}i} \\ \sum_{i=1, i\neq l}^{N} T_{il} \Delta f_l \end{bmatrix}. \tag{4}$$

Moreover, considering that the frequency control system is a sampling control system under the edge computing framework essentially, the respective discrete-time model with the sampling time T_{s} is given by

$$\begin{cases} X_i(k+1) = E_i X_i(k) + F_i u_i(k) + G_i w_i(k), \\ Y_i(k) = C_i X_i(k), \end{cases} \tag{5}$$

where $E_i = e^{A_i T_{\text{s}}}$, $F_i = \int_0^{T_{\text{s}}} e^{A_i t} dt B_i$, and $G_i = \int_0^{T_{\text{s}}} e^{A_i t} dt H_i$.

3. Transmission Delay Analysis in Edge Computing Environment

Generally, the total time delay during the transmission process from the underlying participating equipment to the edge computing device includes the following three parts: serial delay, propagation delay, and routing delay [16]. Hence, the following equation holds.

$$\tau_{\Sigma} = \tau_{\text{serial}} + \tau_{\text{propagation}} + \tau_{\text{routing}}, \tag{6}$$

where τ_{Σ} is the total time delay. Besides, the serial delay (τ_{serial}) is proportional to the size of packets (denoted as P_{size}) and inversely proportional to the transmission rate (denoted as $D_{\text{transmission}}$). The propagation delay is proportional to the transmission distance (denoted as Length_{Σ}) and inversely proportional to the propagation velocity (denoted as V) in a certain physical media. Obviously, both of the serial delay and propagation delay are constants and can be calculated by the following equations.

$$\begin{aligned} \tau_{\text{serial}} &= \frac{P_{\text{size}}}{D_{\text{transmission}}}, \\ \tau_{\text{propagation}} &= \frac{\text{Length}_{\Sigma}}{V}. \end{aligned} \tag{7}$$

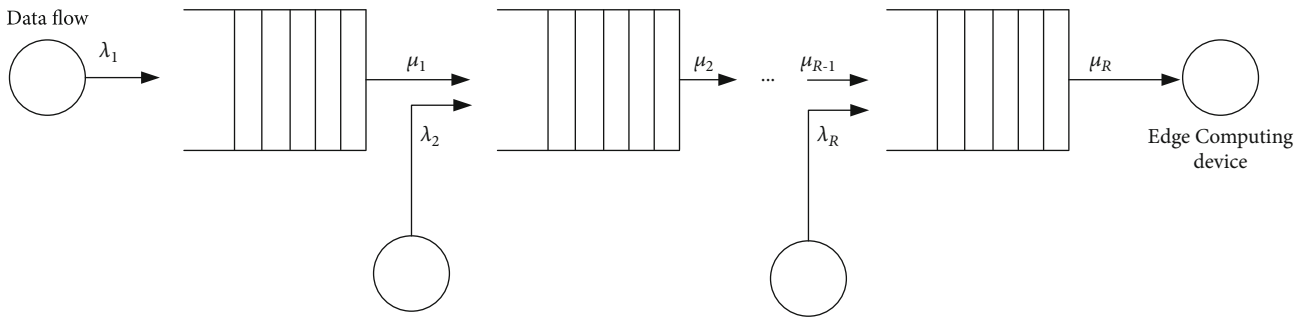

Figure 3: Multihop transmission model in edge computing environment.

In particular, the uncertain routing delay is caused by the queuing and forwarding of multiple data flows in the switches. Specifically, as shown in Figure 3, the operating statuses transmitted from the underlying equipment to the edge computing device need to pass through multiple switches with limited forward capacities. Therefore, at the entrance of a switch, the data flows from different receivers form a queue. Such queuing process can be described as a cascade M/M/1 model based on the queuing theory [21].

Let μ_r denote the forwarding rate of the r-th ($r = 1, 2, \cdots, R$) switch provided for the data flow and τ_r denote the queuing delay of the data flow transmitted by the r-th switch. Assume that a data flow passes through the switches numbered as $1, 2, \cdots, R$ in turn and the data arrival process at the r-th switch obeys the Poisson process with parameter λ_r. Based on the queuing theory, the probability density function (PDF) of the queuing delay at the r-th switch satisfies

$$g(\tau_r) = (\mu_r - \lambda_r)e^{-(\mu_r-\lambda_r)\tau_r}, \quad \tau_r > 0. \tag{8}$$

The corresponding cumulative distribution function (CDF) is given by

$$\bar{g}(\tau_r) = \int_0^{\tau_r} g(t)dt = 1 - e^{-(\mu_r-\lambda_r)\tau_r}, \quad \tau_r > 0. \tag{9}$$

It can be seen that the queuing delay in r-th switch satisfies an exponential distribution with the parameter $\mu_r - \lambda_r$. Furthermore, when the switches $1 - R$ are independent to each other, the total routing delay (τ_{routing}) satisfies

$$\tau_{\text{routing}} = \sum_{r=1}^{R} \tau_r. \tag{10}$$

The corresponding PDF and CDF are given by Equations (11) and (12), respectively.

$$g(\tau_{\text{routing}}) = \prod_{r=1}^{R}(\mu_r - \lambda_r)e^{-\sum_{r=1}^{R}(\mu_r-\lambda_r)\tau_r}, \quad \tau_r > 0, \tag{11}$$

$$\bar{g}(\tau_{\text{routing}}) = \prod_{r=1}^{R}\left(1 - e^{-(\mu_r-\lambda_r)\tau_r}\right), \quad \tau_r > 0. \tag{12}$$

Finally, considering that the serial delay and propagation delay are constants, the PDF and CDF of the total transmission delay (τ_Σ) in the proposed edge computing environment equate to those of the total routing delay (τ_{routing}).

4. Dynamic Characteristic Analysis of Closed-Loop Frequency Control System with Time Delay and Packet Loss

In this paper, to economize the memory space of edge computing devices, each microgrid adopts the memoryless state-feedback control mode, as shown in

$$u_i(k) = K_i X_i^{\text{newest}}(k), \tag{13}$$

where K_i is the controller gain and $X_i^{\text{newest}}(k)$ is the newest packet arrived at the edge computing device.

Noting that the total transmission delay (τ_Σ) always satisfies $\tau_\Sigma \le LT_s (L \in \mathbf{Z}^+)$, in this paper, LT_s is defined as the preset maximum transmission delay. In other words, if the transmission delay of a packet is less than LT_s, then this packet is called an effective packet and will be used to generate the control instructions $u_i(k)$. Otherwise, if the transmission delay of a packet exceeds LT_s, this packet is viewed as a dropped one and will not be used to generate the control instruction $u_i(k)$. Obviously, the different transmission delay may cause that the edge computing device use different packets to generate the control instructions. Hence, the corresponding dynamic characteristics of closed-loop frequency control system will switch with the varying time delays.

Without loss of generality, let p_v and p_{v+1} be the serial number of the two neighbouring effective packets sampled at $t = p_v T_s$ and $t = p_{v+1} T_s$. Both the two packets are used to generate the control instructions due to the fact that their transmission delays are within $[0, LT_s]$. Obviously, the packets sampled within $((p_v + 1)T_s, p_v T_s)$ are dropped due to the transmission delays exceeding LT_s. The maximum number of consecutive dropped packets can be denoted as $D_{\max} = \max(p_{v+1} - p_v)$. Then, the dynamics of closed-loop frequency control system during any two neighbouring effective packets (i.e., $t \in [p_v T_s, p_{v+1} T_s)$) can be described as a switching model dependent on the time-varying delays. In order to clearly illustrate the modelling process for the closed-loop frequency control system with time delay and packet loss, in this section, we take $L = 1$ as an example. As shown in Figure 4, there are two possible scenarios of the closed-loop frequency control system with varying time delays.

Scenario 1: $\tau_\Sigma = 0$, i.e., the packets sampled at $t = p_v T_s$ arrive at the edge computing device without any delay. Therefore, the newest packet satisfies $X_i^{\text{newest}}(k) = X_i(p_v)$, t

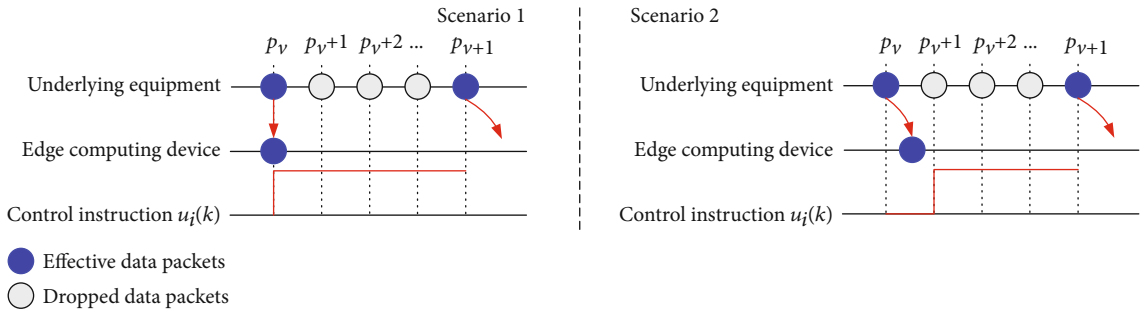

Figure 4: Effects of time delays on the closed-loop frequency control system.

$\in [p_v T_s, p_{v+1} T_s)$. According to the discrete-time model of frequency control system (i.e., Equation (5)), the dynamics of close-loop frequency control systems during the time interval $[p_v T_s, p_{v+1} T_s)$ can be derived as follows:

$$\begin{cases} X_i(p_v+1) = (E_i + F_i K_i) X_i(p_v) + G_i w_i(p_v), \\ X_i(p_v+2) = (E_i + F_i K_i) X_i(p_v+1) + G_i w_i(p_v+1) = \left(E_i^2 + E_i F_i K_i + F_i K_i\right) X_i(p_v) + E_i G_i w_i(p_v) + G_i w_i(p_v+1), \\ \vdots \\ X_i(p_{v+1}) = \left(E_i^{D_{\max}+1} + \sum_{\xi=0}^{D_{\max}} E_i^{\xi} F_i K_i\right) X_i(p_v) + \sum_{\xi=0}^{D_{\max}} E_i^{D_{\max}-\xi} G_i w_i(p_v+\xi). \end{cases} \tag{14}$$

Scenario 2: $\tau_\Sigma \le 1 \times T_s$, i.e., the packet sampled at $t = p_v T_s$ is transmitted to the edge computing device with a delay less than $1 \times T_s$. In this scenario, the control instruction during the time interval $[p_v T_s, p_{v+1} T_s)$ satisfies the following piecewise function

$$X_i^{\text{newest}}(k) = \begin{cases} X_i(p_{v-1}), p_v T_s \le t < (p_v+1) T_s, \\ X_i(p_v), (p_v+1) T_s \le t < p_{v+1} T_s. \end{cases} \tag{15}$$

Similar to Scenario 1, the dynamics of close-loop frequency control systems during the time interval $[p_v T_s, p_{v+1} T_s)$ can be derived as follows:

$$X(p_{v+1}) = \left(E_i^{D_{\max}+1} + \sum_{\xi=0}^{D_{\max}-1} E_i^{\xi} F_i K_i\right) X_i(p_v) + E_i^{D_{\max}} F_i K_i X_i(p_{v-1}) + \sum_{\xi=0}^{D_{\max}} E_i^{D_{\max}-\xi} G_i w_i(p_v+\xi). \tag{16}$$

More generally, the above derivation process in this section can be extended to case of $L \in \mathbf{N}^+$. Define the following two augmented vectors:

$$\begin{aligned} \bar{X}_i(p_v) &= \left[X_i^{\mathrm{T}}(p_v), X_i^{\mathrm{T}}(p_{v-1}), \cdots, X_i^{\mathrm{T}}(p_{v-L})\right]^{\mathrm{T}}, \\ W_i(p_v) &= \left[w_i^{\mathrm{T}}(p_v), w_i^{\mathrm{T}}(p_v+1), \cdots, w_i^{\mathrm{T}}(p_v+L)\right]^{\mathrm{T}}. \end{aligned} \tag{17}$$

Hence, there exist 2^L possible scenarios of the closed-loop frequency control system in the i-th microgrid, uniformly described by

$$\begin{cases} \bar{X}_i(p_{v+1}) = \underbrace{\begin{bmatrix} E_i^{D_{\max}+1} + \sum_{\xi=0}^{D_{\max}-\zeta} E_i^{\xi} F_i K_i & \sum_{\xi=D_{\max}-\zeta+1}^{\psi_1} E_i^{\xi} F_i K_i & \cdots & \sum_{\xi=D_{\max}-\zeta+l-1}^{\psi_{L-1}} E_i^{\xi} F_i K_i & \sum_{\xi=D_{\max}-\zeta+L}^{\psi_L} E_i^{\xi} F_i K_i \\ I & 0 & \cdots & 0 & 0 \\ 0 & I & \cdots & 0 & 0 \\ \vdots & \vdots & \vdots & \vdots & \vdots \\ 0 & 0 & \cdots & I & 0 \end{bmatrix}}_{\Phi_i^{\xi}} \bar{X}_i(p_v) + \underbrace{\begin{bmatrix} E_i^{D_{\max}} G_i & E_i^{D_{\max}-1} G_i & \cdots & G_i \\ 0 & 0 & \cdots & 0 \\ \vdots & \vdots & \vdots & \vdots \\ 0 & 0 & \cdots & 0 \end{bmatrix}}_{\Lambda_i} W_i(p_v), \\ Y(p_v) = \underbrace{\left[C_i, \underbrace{0, 0, \cdots, 0}_{L}\right]}_{\bar{C}_i} \bar{X}_i(p_v), \end{cases} \tag{18}$$

where $\zeta = \{0, 1, \cdots, L\}$; the values of $\{\Psi_1, \Psi_2, \cdots, \Psi_L\}$ are shown in Equation (19) where the arrow "$\longrightarrow$" represents $\{\Psi_1, \Psi_2, \cdots, \Psi_L\}$ take values from the same row.

$$\begin{array}{cccc} \Psi_1 & & \Psi_2 & \cdots \quad \Psi_L \\ \left[\begin{array}{ccccc} D_{\max}-\zeta+1 & \rightarrow & D_{\max}-\zeta+2 & \rightarrow\cdots & D_{\max}-\zeta+L \\ D_{\max}-\zeta+2 & \rightarrow & D_{\max}-\zeta+3 & \rightarrow\cdots & D_{\max}-\zeta+L+1 \\ \vdots & \rightarrow & & \rightarrow\cdots & \vdots \\ D_{\max}-2 & \rightarrow & D_{\max}-1 & \rightarrow\cdots & D_{\max}-1 \\ & & & & 0 \\ & & & & 0 \\ D_{\max}-1 & \rightarrow & 0 & \rightarrow\cdots & \vdots \quad L-1 \\ & & & & 0 \end{array}\right] \end{array} \tag{19}$$

5. H_∞-Controller Optimization considering Dynamic Performance Improvement

The controller gain K_i not only needs to ensure that the closed-loop frequency control systems are asymptotically stable during any two neighbouring effective packets but also require to have a robust attenuation ability against the external power disturbances from the load demands and renewable outputs. In other words, there exists the following inequality between the output $Y_i(p_v)$ and the external power disturbances $W_i(p_v)$ at any time $t = p_v T_s$.

$$\|Y_i(p_v)\|_2 \le \gamma^2 \|W_i(p_v)\|_2, \tag{20}$$

where γ is the attenuation factor and $\|\cdot\|_2$ is the 2-norm operator. Let $k(p_v)$ and $k(p_{v+1}) \in \{1, 2, \cdots, 2^L\}$ denote the serial numbers of the possible operation scenarios at time $t = p_v T_s$ and $t = p_{v+1} T_s$. A candidate Lyapunov function is constructed by

$$V_i(p_v) = \bar{X}_i^{\mathrm{T}}(p_v) \Omega_{k(p_v)} \bar{X}_i(p_v), \tag{21}$$

where $\Omega_{k(p_v)}$ is a symmetric positive definite matrix. When the state vector of closed-loop frequency control system changes from $\bar{X}_i(p_v)$ to $\bar{X}_i(p_{v+1})$, the increment of Equation (21) is given by

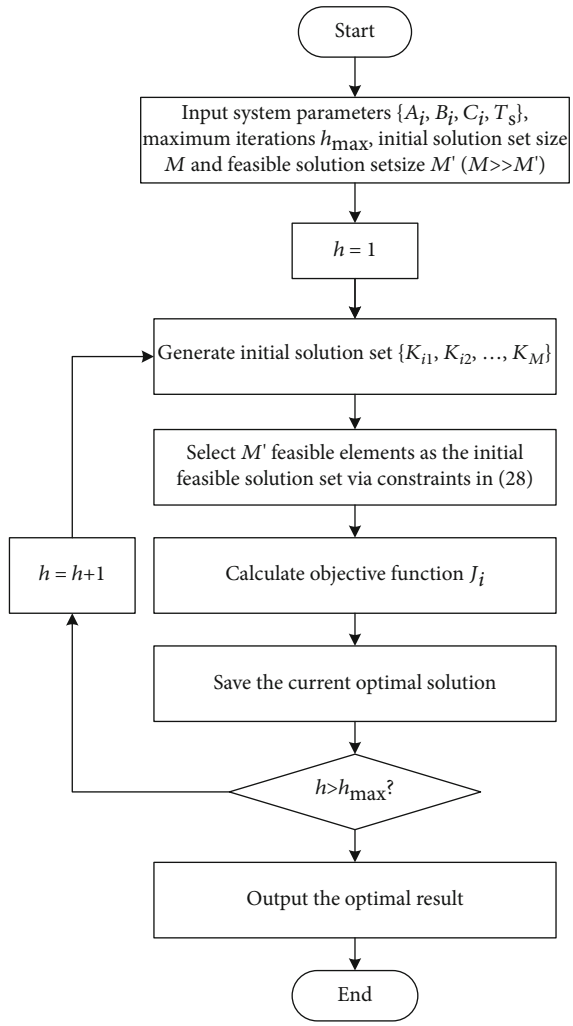

Figure 5: Flowchart for controller gain optimization.

$$\begin{aligned} \Delta V_i(p_v) = V_i(p_{v+1}) - V_i(p_v) = \bar{X}_i^{\mathrm{T}}(p_{v+1}) \Omega_{k(p_{v+1})} \bar{X}_i(p_{v+1}) \\ - \bar{X}_i^{\mathrm{T}}(p_v) \Omega_{k(p_v)} \bar{X}_i(p_v). \end{aligned} \tag{22}$$

Substituting Equation (18) and inequality (20) in Equation (22) results in

$$\begin{aligned} \Delta V_i(p_v) &\le \begin{bmatrix} \bar{X}_i(p_v) \\ W_i(p_v) \end{bmatrix}^{\mathrm{T}} \begin{bmatrix} \left(\Phi_i^{\zeta}\right)^{\mathrm{T}} \Omega_{k(p_v)} \Phi_i^{\zeta} - \Omega_{k(p_{v+1})} & \left(\Phi_i^{\zeta}\right)^{\mathrm{T}} \Omega_{k(p_v)} \Lambda_i \\ * & \Lambda_i^{\mathrm{T}} \Omega_{k(p_v)} \Lambda_i \end{bmatrix} \begin{bmatrix} \bar{X}_i(p_v) \\ W_i(p_v) \end{bmatrix} - Y_i^{\mathrm{T}}(p_v) Y_i(p_v) + \gamma^2 W_i^{\mathrm{T}}(p_v) W_i(p_v) \\ &= \begin{bmatrix} \bar{X}_i(p_v) \\ W_i(p_v) \end{bmatrix}^{\mathrm{T}} \begin{bmatrix} \begin{pmatrix} \left(\Phi_i^{\zeta}\right)^{\mathrm{T}} \Omega_{k(p_v)} \Phi_i^{\zeta} - \Omega_{k(p_{v+1})} \\ + \bar{C}_i^{\mathrm{T}} \bar{C}_i \end{pmatrix} & \left(\Phi_i^{\zeta}\right)^{\mathrm{T}} \Omega_{k(p_v)} \Lambda_i \\ * & \Lambda_i^{\mathrm{T}} \Omega_{k(p_v)} \Lambda_i - \gamma^2 I \end{bmatrix} \begin{bmatrix} \bar{X}_i(p_v) \\ W_i(p_v) \end{bmatrix}, \end{aligned} \tag{23}$$

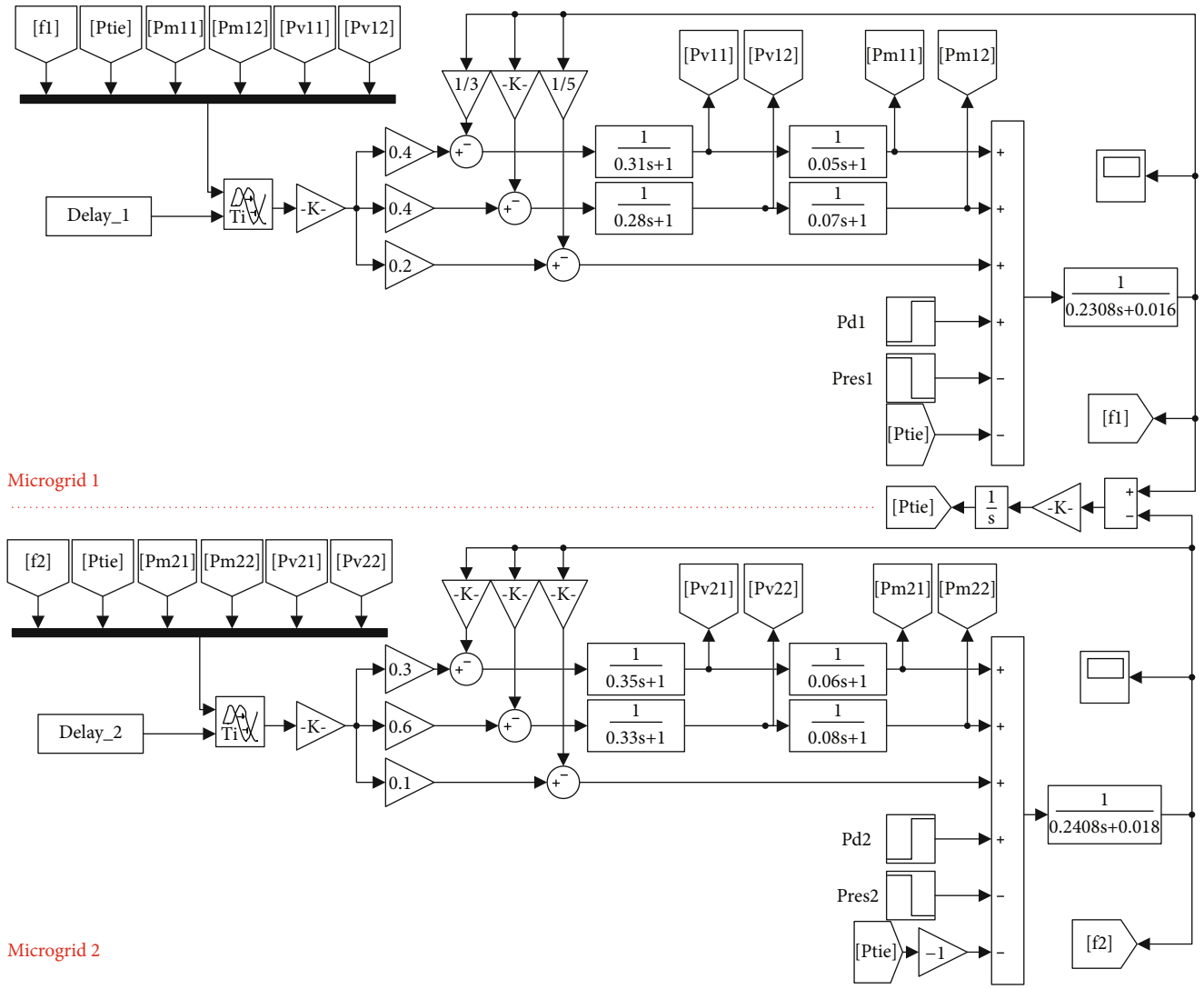

FIGURE 6: Simulation diagram of multi-microgrids.

where I is an identity matrix with suitable dimensions. When the following matrix inequality

$$\begin{bmatrix} \begin{pmatrix} \left(\Phi_i^{\zeta}\right)^{\mathrm{T}} \Omega_{k(p_v)} \Phi_i^{\zeta} - \Omega_{k(p_{v+1})} \\ +\bar{C}_i^{\mathrm{T}} \bar{C}_i \end{pmatrix} & \left(\Phi_i^{\zeta}\right)^{\mathrm{T}} \Omega_{k(p_v)} \Lambda_i \\ * & \Lambda_i^{\mathrm{T}} \Omega_{k(p_v)} \Lambda_i - \gamma^2 I \end{bmatrix} < 0 \tag{24}$$

holds, the integral of Lyapunov function on $[0, +\infty)$ with zero initial conditions satisfies

$$\begin{aligned} 0 \le V_i(+\infty) - V_i(0) &\le \sum_{p_v=0}^{+\infty} \left(-Y_i^{\mathrm{T}}(p_v) Y_i(p_v) + \gamma^2 W_i^{\mathrm{T}}(p_v) W_i(p_v)\right) \\ &= -\|Y_i(p_v)\|_2 + \gamma^2 \|W_i(p_v)\|_2. \end{aligned} \tag{25}$$

Overall, if the matrix inequality (24) holds, the control gain K_i can guarantee the closed-loop frequency control system has the asymptotic stability in the case of stochastic communication changes and H_∞-robust attenuation performance against external power disturbances simultaneously.

Besides, in order to improve the dynamic performance during frequency restoration process, the integral of absolute error (IAE) of the frequency is chosen as the objective function, as shown in Equation (26). The IAE of frequency reflects the transient response performance of the frequency control system to external power disturbances

$$J_i = \sum_{k=0}^{\infty} |\Delta f_i(k)|. \tag{26}$$

In conclusion, a constrained optimization model for the controller gain K_i is established, as follows.

$$\begin{cases} \text{objective}: \ \min \ J_i \\ \text{s.t.}: \ \begin{cases} \begin{bmatrix} \left(\left(\Phi_i^{\zeta}\right)^{\mathrm{T}}\Omega_{k(p_v)}\Phi_i^{\zeta} - \Omega_{k(p_{v+1})}\right) + \bar{C}_i^{\mathrm{T}}\bar{C}_i & \left(\Phi_i^{\zeta}\right)^{\mathrm{T}}\Omega_{k(p_v)}\Lambda_i \\ * & \Lambda_i^{\mathrm{T}}\Omega_{k(p_v)}\Lambda_i - \gamma^2 I \end{bmatrix} < 0 \\ \Omega_{k(p_r)} = \Omega_{k(p_r)}^{\mathrm{T}} > 0, \Omega_{k(p_{r+1})} = \Omega_{k(p_{r+1})}^{\mathrm{T}} > 0. \end{cases} \end{cases} \tag{27}$$

According to Equation (18), the matrix Φ_i^{ζ} contains the controller gain K_i which needs to be optimized. Besides, there exists a multiplicative relation between matrix Φ_i^{ζ} and unknown matrix $\Omega_{k(p_v)}$. Therefore, the constraints (27) do not satisfy the linear matrix inequality (LMI) forms and cannot be solved by directly using the robust control toolbox of MATLAB directly. In this paper, an iterative relaxation technology combined with heuristic search method is proposed to optimize the controller gain K_i. The flowchart is shown in Figure 5. Firstly, an initial solution set containing considerable matrixes with the same dimensions of K_i is generated randomly. Then, the initial feasible solution set is selected from the initial solution set according to the constraints in (27). Secondly, the initial solution set is updated via the operations such as mutation and pheromone update. The constraints (27) are used again to select the feasible solution set for the next iteration. Since the candidates in initial solution set for K_i are fixed during the whole optimization process, the matrix nonlinear matrix inequality in (27) is relaxed into the LMIs.

6. Simulations and Discussions

In this section, the feasibility of the proposed cascade M/M/1 model for communication network in edge computing framework is verified by using OPNET Modeler 14.5. In addition, assume that the number of microgrids in the multi-microgrid is 2 and each microgrid contains two synchronous generators and one energy storage system. The frequency control in multi-microgrid is simulated in MATLAB/Simulink environment, as shown in Figure 6. The time delays during the simulation process adopt the simulation results obtained from the OPNET. The controller gain is obtained according to the optimization algorithm proposed in Section 5 where the particle swarm optimization method is used. The synchronization coefficient between the two microgrids satisfies $T_{12} = T_{21} = 0.52$ p.u./Hz. Besides, the communication system configurations in both two microgrids are assumed to be the same. To evaluate the dynamic performance of the proposed control strategy, the step changes of renewable output and load demand with 0.1 p.u. and -0.1 p.u. occur at $t = 0$ s in each microgrid. Other simulation parameters are demonstrated in Table 1.

6.1. Transmission Delays in Edge Computing Framework. As shown in Figure 7, a multihop data transmission network is established in OPNET environment to verify the proposed cascade M/M/1 model for time delay calculation under the edge computing framework. It should be noted that since the number of transmission hops is equal to the number of forwarding nodes, a chain topology is adopted in the simulation. Figure 8 shows the statistical results of transmission delays of 100 consecutive packets and the theoretical mean value of time delays calculated by the proposed M/M/1 model.

According to Figure 8, the simulation mean value of the transmission delays is 10.15 ms. Meanwhile, the theoretical mean value calculated by the proposed cascade M/M/1 model is 11.41 ms. The relative error between theoretical and simulation values is 11.04%. Therefore, the simulation results illustrate that the proposed cascade M/M/1 model can effectively reflect the transmission characteristics in edge computing environment. In addition, it can be found that the number of continuous packets with transmission delays exceeding 20 ms is less than 3. Therefore, in controller design process, the preset maximum transmission delay is assumed

Table 1: Simulation parameters.

Parameters	Values	Illustrations
T_{g11} (s)	0.31	Microgrid 1
T_{t11} (s)	0.05	
T_{g12} (s)	0.28	
T_{t12} (s)	0.07	
R_{11} (Hz/p.u.)	3	
R_{12} (Hz/p.u.)	2.8	
R_{ESS_11} (Hz/p.u.)	5	
M_{eq_1} (p.u. s)	0.2308	
D_{eq_1} (p.u./Hz)	0.016	
$(\alpha_{11}, \alpha_{12}, \beta_{11})$	(0.4, 0.4, 0.2)	
T_{g21} (s)	0.35	Microgrid 2
T_{t21} (s)	0.06	
T_{g22} (s)	0.33	
T_{t22} (s)	0.08	
R_{21} (Hz/p.u.)	2.87	
R_{22} (Hz/p.u.)	2.5	
R_{ESS_21} (Hz/p.u.)	4.5	
M_{eq_2} (p.u. s)	0.2408	
D_{eq_2} (p.u./Hz)	0.018	
$(\alpha_{21}, \alpha_{22}, \beta_{21})$	(0.3, 0.6, 0.1)	
T_s (ms)	10	Communication networks
P_{size} (bits)	200	
$D_{transmission}$ (Mbps)	10	
Length_{Σ} (km)	50	
V (km/s)	1.8×10^5	
λ_r (packet/s)	50	
μ_r (packet/s)	500	
R	5	

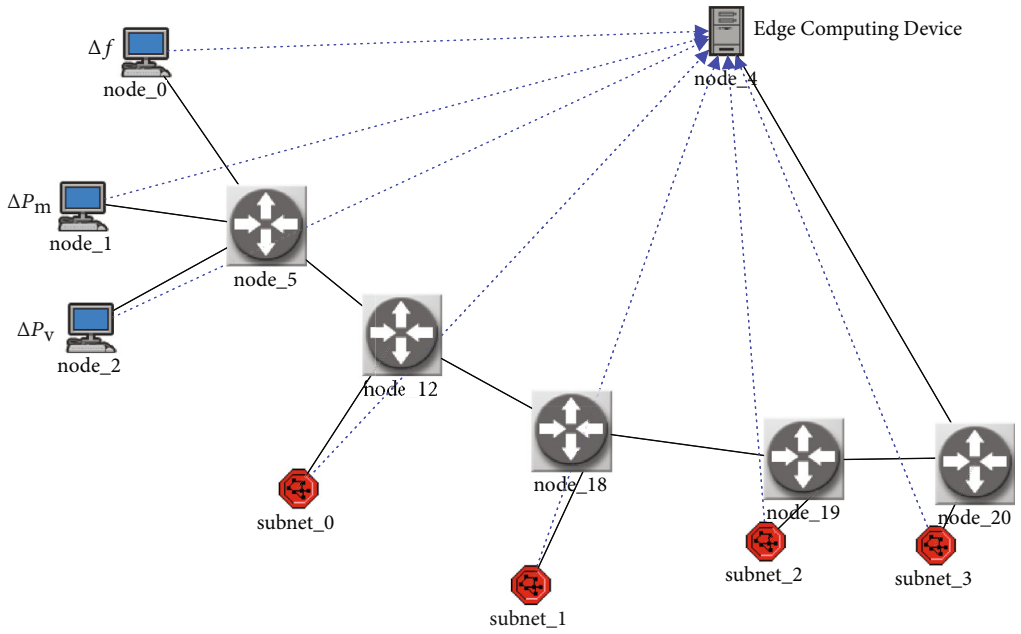

Figure 7: Schematic diagram of communication network in edge computing framework.

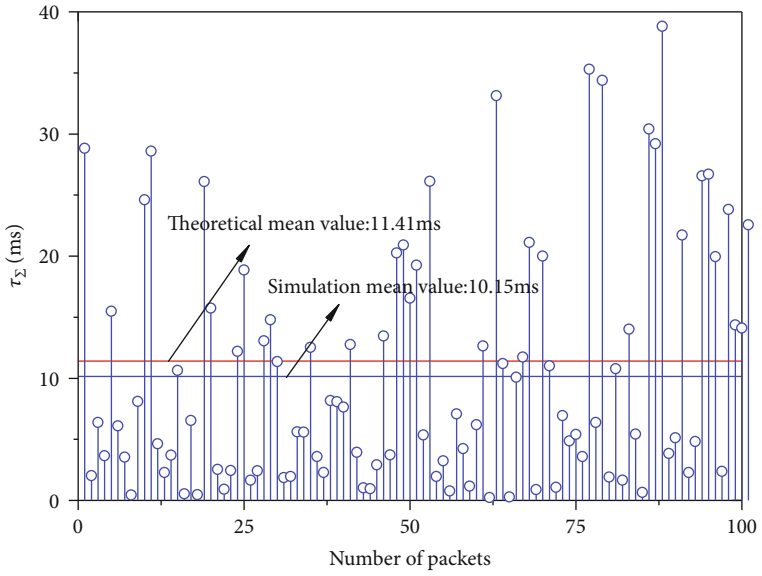

Figure 8: Statistical results of transmission delays of 100 consecutive packets in edge computing environment.

to be 20 ms (i.e., 2×10 ms) while the maximum number of consecutive dropped packets (i.e., $D_{\max}$) is assumed to be 3.

6.2. Control Performance Analysis with the Proposed Method

6.2.1. Comparisons with the Traditional Centralized Control Scheme. In the traditional centralized control schemes, all the operation statuses of the microgrids should be transmitted to the only control center in the whole power system. Without loss of generality, the simplest case that there is only one switch between the edge computing device and the control center is considered in this subsection, as shown in Figure 9. Figure 10 shows the statistical results of transmission delays of 100 consecutive packets and the theoretical mean value of time delays calculated by the proposed M/M/1 model. According to Figure 10, the number of continuous packets with transmission delays which exceeds 20 ms is less than 6. Therefore, the preset maximum transmission delay is assumed to be 20 ms (i.e., 2×10 ms) while the maximum number of consecutive dropped packets (i.e., $D_{\max}$) is assumed to be 6. In addition, in order to quantitatively evaluate the control performance, the following indexes are selected:

(1) Peak value of frequency deviation: the maximum value of the absolute value of frequency deviation when step changes of external power disturbances occur

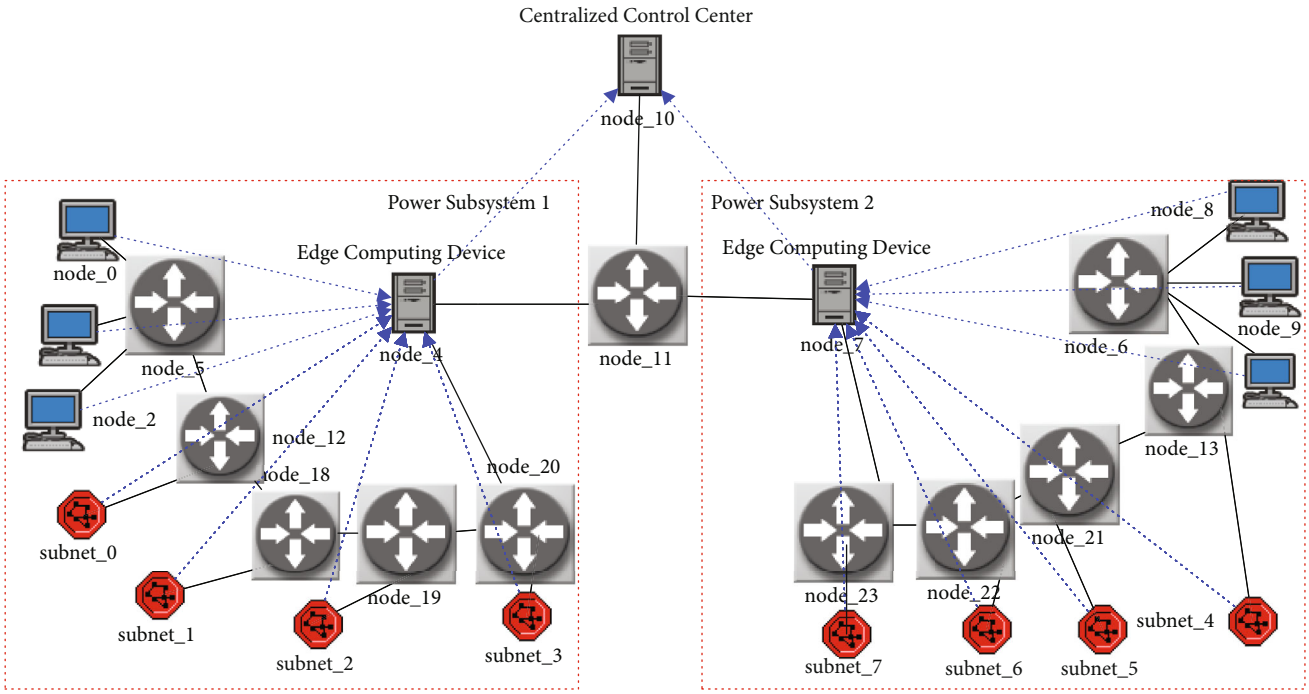

Figure 9: Schematic diagram of communication network in traditional centralized framework.

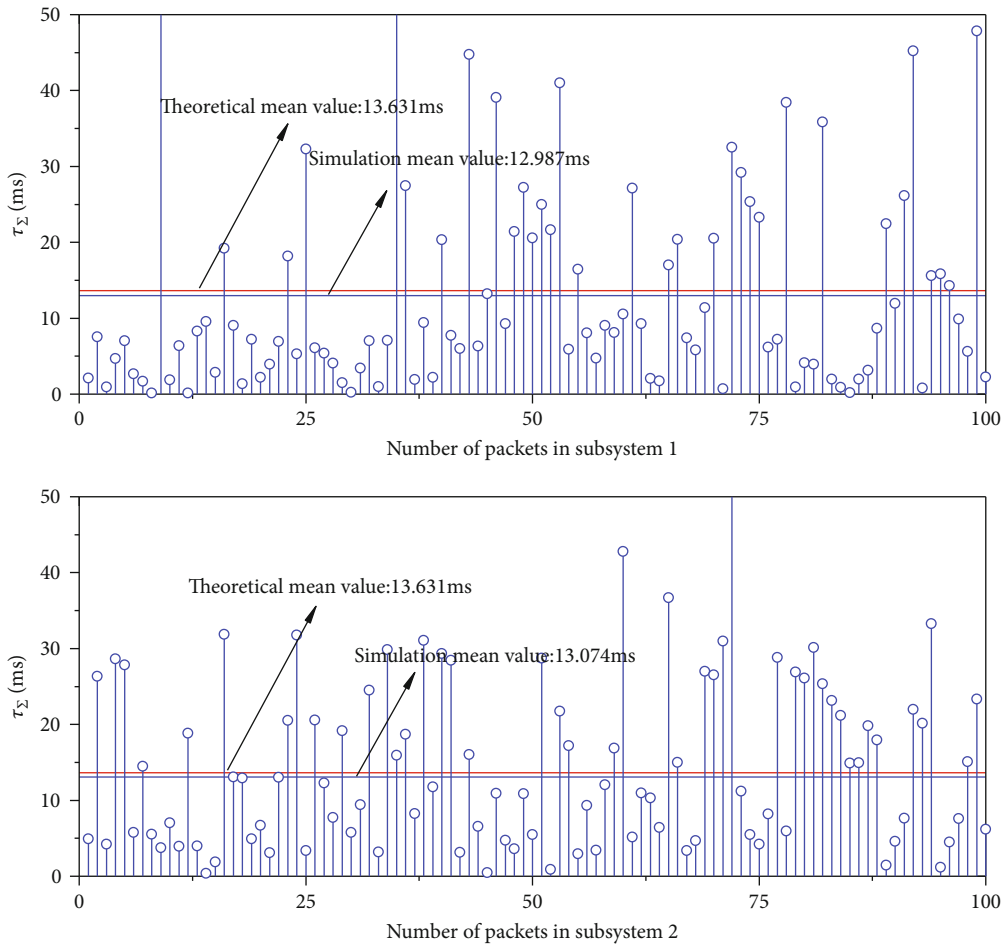

Figure 10: Statistical results of transmission delays of 100 consecutive packets in traditional centralized framework.

Table 2: Performance indexes with traditional centralized framework and proposed edge computing framework.

Microgrids	Control strategies	Peak value (Hz)	Restoration time (s)	IAE (Hz)
1	This paper	0.0164	1.36	0.4182
	Centralized framework	0.0243	1.14	0.6092
2	This paper	0.0209	2.01	0.8920
	Centralized framework	0.0370	4.27	3.5346

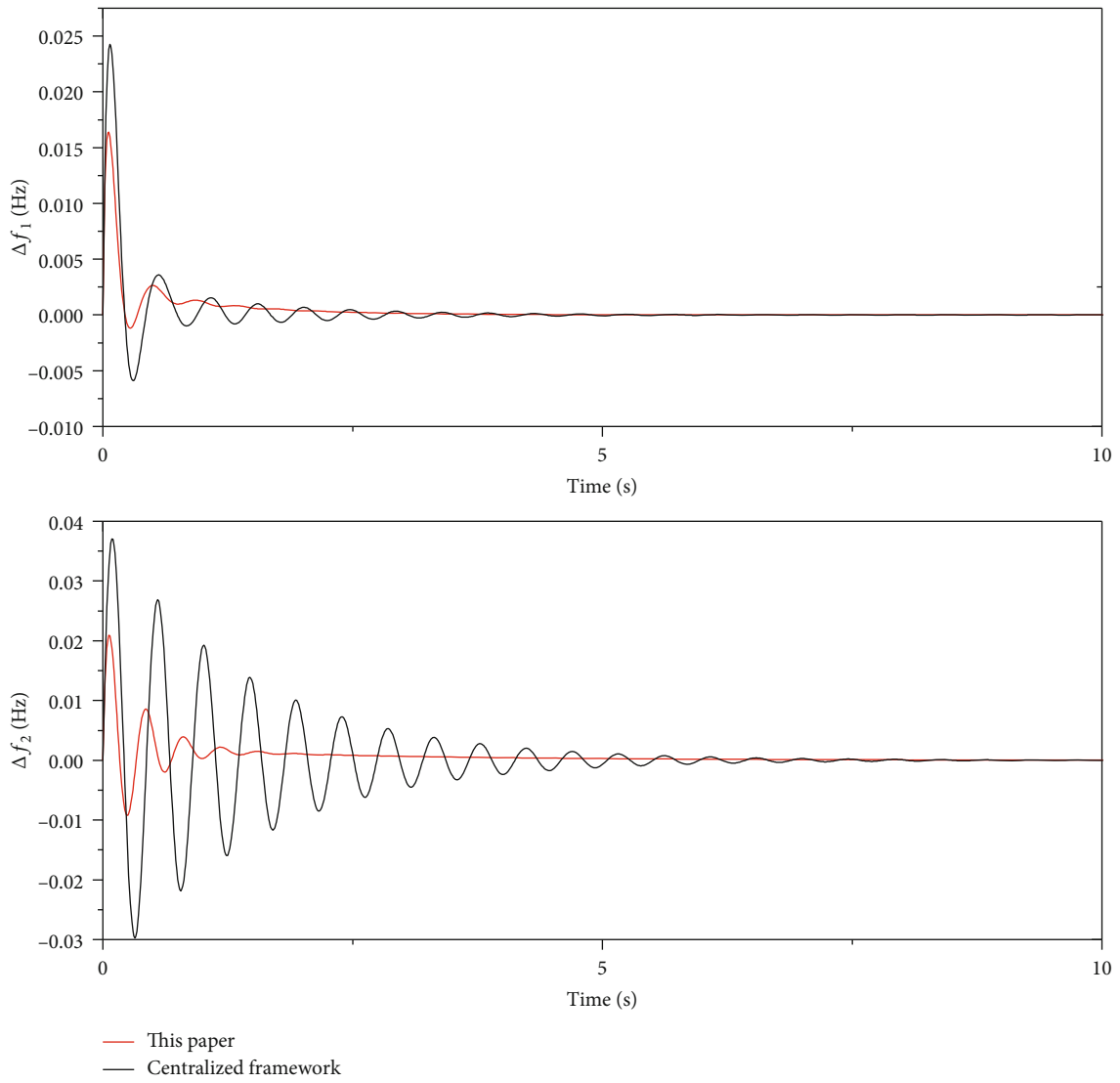

Figure 11: Frequency deviations with traditional centralized framework and proposed edge computing framework.

(2) Restoration time of frequency deviation: the starting time when the frequency deviation restores and maintains within ±5% of the peak value

(3) IAE of the frequency: the result calculated according to Equation (26)

In this subsection, the controller gains of both centralized scheme and edge computing framework are obtained with the proposed H_∞-switching control method in Section 5. Figure 10 shows the frequency deviation responses with the traditional centralized and the proposed edge computing framework. Table 2 demonstrates the corresponding performance indexes. For the first microgrid, according to Figures 10 and 11 and Table 2, although the restoration times of the two control schemes are close, the peak value of our proposed edge computing framework is reduced by 32.51% compared with the traditional centralized control scheme. Meanwhile, for the second microgrid, not only the peak value of our proposed edge computing framework is reduced by

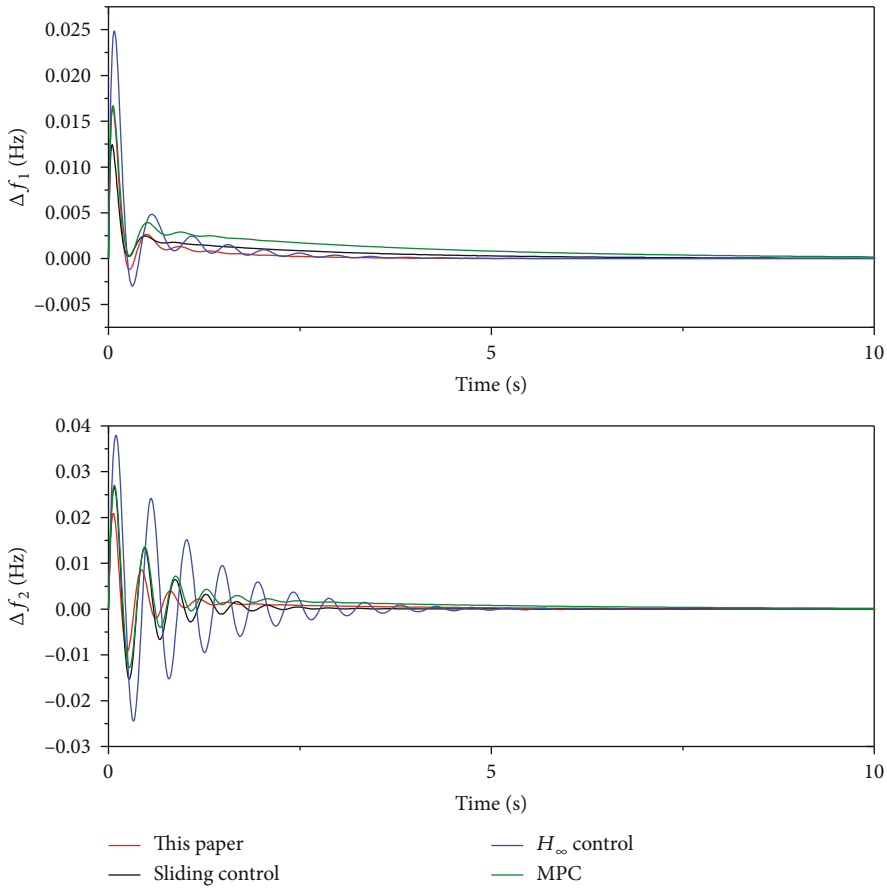

Figure 12: Frequency deviations with different control strategies.

Table 3: Performance indexes with different control strategies.

Microgrids	Control strategies	Peak value (Hz)	Restoration time (s)	IAE (Hz)
1	This paper	0.0164	1.36	0.4182
	Sidling control	0.0124	3.26	0.6658
	H_∞ control	0.0248	1.65	0.7259
	MPC	0.0167	4.95	1.3294
2	This paper	0.0209	2.01	0.8920
	Sidling control	0.0266	1.73	1.0061
	H_∞ control	0.0380	2.93	2.4598
	MPC	0.0270	3.31	1.6974

43.51% but also the corresponding restoration time can be shortened by 52.93% compared with the centralized control scheme. In addition, the IAEs in both two microgrids using the proposed edge computing framework are less than the results using the centralized scheme. The simulation results show that the proposed edge computing framework can provide a better frequency deviation damping performance. This is because the proposed control strategy based on edge computing framework only requires the local operation statuses and the edge computing device which is closer to the underlying participating equipment. Hence, compared with the traditional centralized control scheme, the communication network with edge computing framework can provide a higher quality of service (QoS) for the data flows and has the less consecutive dropped packets.

6.2.2. Comparisons with Different Controller Design Methods in Edge Computing Framework. In this subsection, the superiority of dynamic performance with our proposed H_∞-switching control strategy compared with other design methods is discussed. The comparison methods are as follows: (1) H_∞ control strategy in [9]; (2) MPC strategy in [17]; (3) sliding control strategy in [18]. All the control strategies in this subsection adopt the decentralized scheme and can be applied into the edge computing framework.

Figure 12 shows the frequency deviation responses with different controller design methods. Table 3 demonstrates corresponding dynamic performance indexes. For the first microgrid, according to Figure 12 and Table 3, compared with the sliding control strategy, the maximum frequency deviation with our proposed H_∞-switching control is 32.3% larger while the restoration time is shortened by 58.28%. Compared with H_∞ control, the maximum frequency deviation and restoration time are reduced by 33.87% and 17.58%, respectively. Compared with the MPC method, the maximum frequency deviation and restoration time are reduced by 1.80% and 72.53%, respectively. Note that the IAE of frequency with the proposed H_∞-switching control is reduced by 37.19%, 42.40%, and 68.54%, respectively, compared with the sliding control, H_∞ control, and MPC. Similar results can be obtained for the second microgrid. The reason is that our proposed controller design method optimizes the dynamic performance during frequency restoration process on the premise of ensuring the asymptotical stability of the closed-loop frequency control systems. Therefore, the shorter restoration time and better transition process can be obtained.

7. Conclusions

In this paper, an edge computing-based control scheme is proposed to deal with the frequency stability problem in multi-microgrids. Different from the traditional centralized scheme, the edge computing device is set up in each microgrid to realize the local frequency stability with higher QoS for data transmission and the lower computation burden for controller design. Via describing the closed-loop frequency control system as a delay-dependent switching model, the constraints of controller gain guaranteeing asymptotic stability and H_∞-attenuation performance are strictly derived. Moreover, an optimization algorithm is proposed aiming at improving the transition performance during frequency restoration process. Simulation results show that our proposed method has shorter restoration time in stochastic time delay and packet loss cases. Further researches will focus on the frequency stability problem in edge computing framework suffering from malicious network attacks.

Data Availability

The data used to support the findings of this study are included within the article.

Conflicts of Interest

The authors declare that there is no conflict of interest regarding the publication of this paper.

Acknowledgments

This paper was supported by the Science and Technology Project of State Grid Hebei Electric Power Co. LTD. (B104DY200299).

References

[1] A. Jafari, H. G. Ganjehlou, T. Khalili, and A. Bidram, "A fair electricity market strategy for energy management and reliability enhancement of islanded multi-microgrids," *Applied Energy*, vol. 270, p. 115170, 2020.

[2] B. Wang, Q. Sun, R. Han, and D. Ma, "Consensus-based secondary frequency control under denial-of-service attacks of distributed generations for microgrids," *Journal of the Franklin Institute*, vol. 358, no. 1, pp. 114–130, 2021.

[3] M. M. Esfahani, A. Hariri, and O. A. Mohammed, "A multiagent-based game-theoretic and optimization approach for market operation of multimicrogrid systems," *IEEE Transactions on Industrial Informatics*, vol. 15, no. 1, pp. 280–292, 2019.

[4] T. Yang, Y. Zhang, Z. Wang, and H. Pen, "Secondary frequency stochastic optimal control in independent microgrids with virtual synchronous generator-controlled energy storage systems," *Energies*, vol. 11, no. 9, p. 2388, 2018.

[5] D. E. Olivares, A. Mehrizi-Sani, A. H. Etemadi et al., "Trends in microgrid control," *IEEE Transactions on Smart Grid*, vol. 5, no. 4, pp. 1905–1919, 2014.

[6] L. Yin, T. Yu, B. Yang, and X. Zhang, "Adaptive deep dynamic programming for integrated frequency control of multi-area multi-microgrid systems," *Neurocoputing*, vol. 344, pp. 49–60, 2018.

[7] W. Liu, W. Gu, W. Sheng, X. Meng, Z. Wu, and W. Chen, "Decentralized multi-agent system-based cooperative frequency control for autonomous microgrids with communication constraints," *IEEE Transactions on Sustainable Energy*, vol. 5, no. 2, pp. 446–456, 2014.

[8] X. Liu, H. Nong, K. Xi, and X. Yao, "Robust distributed model predictive load frequency control of interconnected power system," *Mathematical Problems in Engineering*, vol. 2013, 10 pages, 2013.

[9] H. R. Baghaee, M. Mirsalim, G. B. Gharehpetian, and H. A. Talebi, "A generalized descriptor-system robust H_∞ control of autonomous microgrids to improve small and large signal stability considering communication delays and load nonlinearities," *International Journal of Electrical Power & Energy Systems*, vol. 92, pp. 63–82, 2017.

[10] J. Pahasa and I. Ngamroo, "PHEVs bidirectional charging/-discharging and SoC control for microgrid frequency stabilization using multiple MPC," *IEEE Transactions on Smart Grid*, vol. 6, no. 2, pp. 526–533, 2015.

[11] T. Yang, Y. Zhang, W. Li, and A. Y. Zomaya, "Decentralized networked load frequency control in interconnected power systems based on stochastic jump system theory," *IEEE Transactions on Smart Grid*, vol. 11, no. 5, pp. 4427–4439, 2020.

[12] K. S. Ko and D. K. Sung, "The effect of EV aggregators with time-varying delays on the stability of a load frequency control system," *IEEE Transactions on Power Systems*, vol. 33, no. 1, pp. 669–680, 2018.

[13] L. Xiong, H. Li, and J. Wang, "LMI based robust load frequency control for time delayed power system via delay margin estimation," *International Journal of Electrical Power & Energy Systems*, vol. 100, no. 1, pp. 91–103, 2018.

[14] Ş. Sönmez, S. Ayasun, and C. O. Nwankpa, "An exact method for computing delay margin for stability of load frequency control systems with constant communication delays," *IEEE Transactions on Power Systems*, vol. 31, no. 1, pp. 370–377, 2016.

[15] S. Wen, X. Yu, Z. Zeng, and J. Wang, "Event-triggering load frequency control for multiarea power systems with communication delays," *IEEE Transactions on Industrial Electronics*, vol. 63, no. 2, pp. 1308–1317, 2016.

[16] V. P. Singh, N. Kishor, and P. Samuel, "Load frequency control with communication topology changes in smart grid," *IEEE Transactions on Industrial Informatics*, vol. 12, no. 5, pp. 1943–1952, 2016.

[17] P. Ojaghi and M. Rahmani, "LMI-based robust predictive load frequency control for power systems with communication delays," *IEEE Transactions on Power Systems*, vol. 32, no. 5, pp. 4091–4100, 2017.

[18] X. Su, X. Liu, and Y. Song, "Event-triggered sliding-mode control for multi-area power systems," *IEEE Transactions on Industrial Electronics*, vol. 64, no. 8, pp. 6732–6741, 2017.

[19] G. Zhang, C. Li, D. Qi, and H. Xin, "Distributed estimation and secondary control of autonomous microgrid," *IEEE Transactions on Power Systems*, vol. 32, no. 2, pp. 989–998, 2017.

[20] M. Varzaneh, A. Rajaei, A. Jolfaei, and M. Khosravi, "A high step-up dual-source three-phase inverter topology with decoupled and reliable control algorithm," *IEEE Transactions on Industry Applications*, vol. 56, no. 4, pp. 4501–4509, 2020.

[21] J. W. Stahlhut, T. J. Browne, G. T. Heydt, and V. Vittal, "Latency viewed as a stochastic process and its impact on wide area power system control signals," *IEEE Transactions on Power Systems*, vol. 23, no. 1, pp. 84–91, 2008.